Protein kinase D promotes plasticity-induced F-actin stabilization in dendritic spines and regulates memory formation

Norbert Bencsik,[1] Zsófia Szíber,[1] Hanna Liliom,[1] Krisztián Tárnok,[1] Sándor Borbély,[1] Márton Gulyás,[2] Anikó Rátkai,[1] Attila Szűcs,[2] Diána Hazai-Novák,[3] Kornelia Ellwanger,[4] Bence Rácz,[3] Klaus Pfizenmaier,[4] Angelika Hausser,[4] and Katalin Schlett[1,2]

[1]Department of Physiology and Neurobiology, Eötvös Loránd University, H-1117 Budapest, Hungary
[2]MTA-ELTE-NAP B Neuronal Cell Biology Research Group, H-1117 Budapest, Hungary
[3]Department of Anatomy and Histology, Faculty of Veterinary Science, Szent István University, H-1400 Budapest, Hungary
[4]Institute of Cell Biology and Immunology, University of Stuttgart, D-70569 Stuttgart, Germany

Actin turnover in dendritic spines influences spine development, morphology, and plasticity, with functional consequences on learning and memory formation. In nonneuronal cells, protein kinase D (PKD) has an important role in stabilizing F-actin via multiple molecular pathways. Using in vitro models of neuronal plasticity, such as glycine-induced chemical long-term potentiation (LTP), known to evoke synaptic plasticity, or long-term depolarization block by KCl, leading to homeostatic morphological changes, we show that actin stabilization needed for the enlargement of dendritic spines is dependent on PKD activity. Consequently, impaired PKD functions attenuate activity-dependent changes in hippocampal dendritic spines, including LTP formation, cause morphological alterations in vivo, and have deleterious consequences on spatial memory formation. We thus provide compelling evidence that PKD controls synaptic plasticity and learning by regulating actin stability in dendritic spines.

Introduction

Excitatory inputs in the brain mainly target dendritic spines, which are small actin-rich protrusions formed along neuronal dendrites. It is now widely accepted that synaptic plasticity and memory formation modify the morphology of dendritic spines, including the appearance of new protrusions, as well as rearrangement of already existing synaptic connections (reviewed in Holtmaat and Svoboda (2009) and Yuste (2010)).

The cytoskeleton in spines is formed predominantly by F-actin and serves both as a structural framework to maintain shape and as the principal regulator of protein and vesicular trafficking (Frost et al., 2010; Bosch and Hayashi, 2012). Previous studies have shown that F-actin is highly dynamic in spines (Star et al., 2002; Okamoto et al., 2004) and is regulated by a plethora of signaling pathways (Pontrello and Ethell, 2009; Penzes and Cahill, 2012). Depending on the modulation of input activity or homeostatic regulation, spines can undergo structural changes, e.g., enlargement during long-term potentiation (LTP) or shrinkage during long-term depression, with strict temporal and spatial regulations of actin turnover (Bosch and Hayashi, 2012).

The PKD family of serine/threonine kinases comprises three isoforms in mammals (PKD1–3). PKDs are activated by members of the novel PKC family and are recruited to the plasma membrane or intracellular membranes via binding DAG to achieve full activation (Steinberg, 2012). Activated PKDs can exert various cellular functions, including the regulation of cell motility and invasion (LaValle et al., 2010b; Olayioye et al., 2013). In nonneuronal tumor cells, PKD activity suppresses cell motility by controlling actin dynamics via Slingshot (SSH1), p21-activated kinase 4 (PAK4), or cortactin (reviewed in Olayioye et al. (2013) and references therein).

In the rodent brain, all three PKD isoforms are expressed early in embryonal development (Oster et al., 2006). So far, neuronal PKD activity has been shown to affect dendrite development and maintenance, intracellular transport, and Golgi functions, as well as modulation of transmembrane receptors (Cabrera-Poch et al., 2004; Horton et al., 2005; Bisbal et al., 2008; Czöndör et al., 2009; Wang et al., 2014; Quassollo et al., 2015). In this work, we investigated PKD-mediated effects on dendritic spines and the consequences of altered PKD activity upon evoking different forms of neuronal plasticity and memory formation. We show that endogenous PKDs regulate activity-dependent changes in dendritic spines by regulating F-actin

Correspondence to Katalin Schlett: schlettk@ludens.elte.hu

Abbreviations used in this paper: cLTP, chemical LTP; DI, discrimination index; DOX, doxycycline; EPSP, excitatory postsynaptic potential; HFS, high-frequency stimulation; LTP, long-term potentiation; MF, mossy fiber; POPS, population spike; PSD, postsynaptic density; ROI, region of interest; SC, Schaffer collateral.

The Rockefeller University Press $30.00
J. Cell Biol. Vol. 210 No. 5 771–783
www.jcb.org/cgi/doi/10.1083/jcb.201501114

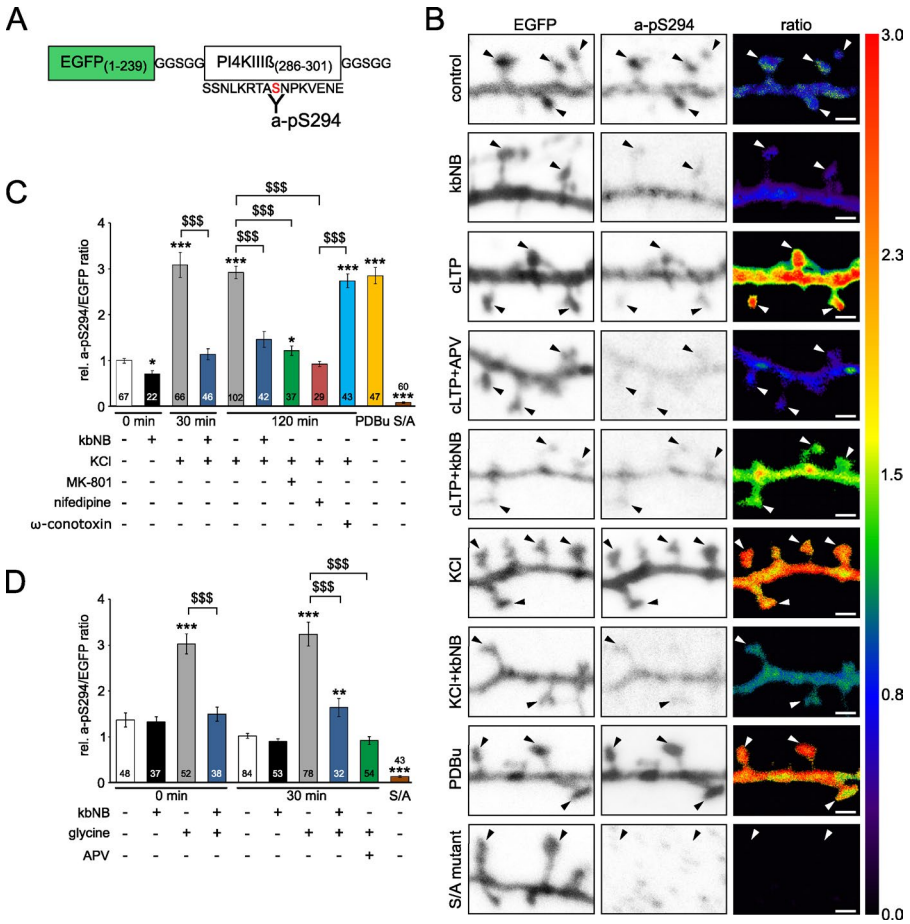

Figure 1. **Endogenous PKD is activated within dendritic spines during plasticity-inducing changes in vitro.** (A) Schematic representation of the PKD activity reporter, containing the PKD-specific substrate sequence of phosphatidylinositol 4-kinase IIIβ (PI4KIIIβ) and the EGFP sequence. The a-pS294 antibody recognizes the phosphorylated Ser294 target site. (B) Inverted fluorescent and a-pS294/EGFP ratio images of tertiary dendritic branches from control or cLTP- or KCl-treated neurons after 30 min. Arrowheads indicate mushroom spines. Bars, 1 µm. (C and D) Relative a-pS294/EGFP ratio values in mushroom spines treated with KCl (C) or cLTP (D) for the indicated time. 3 µM kbNB 142-70 (kbNB) or 1 µM PDBu was applied 1 h before other treatments or for 15 min, respectively. 10 µM MK-801, 50 µM APV, 1 µM nifedipine, and 1 µM ω-conotoxin MVIIC were applied for the indicated time periods. S/A indicates a reporter construct with a nonphosphorylatable alanine mutation. Data were obtained from three to four independent cultures and displayed as mean ± SEM. The number of analyzed spines is indicated within the graphs. Asterisks represent significance compared with control values, and $ symbols indicate significant differences between data pairs. *, $P < 0.05$; **, $P < 0.01$; *** or $$$, $P < 0.001$.

consolidation and provide compelling evidence that PKD activity is required for proper learning and memory formation.

Results

Endogenous PKD is active in dendritic spines

Previously, we have described a PKD activity reporter, which is suitable to visualize endogenous PKD-mediated phosphorylation events in fixed cells (Fig. 1 A; Czöndör et al., 2009; Fuchs et al., 2009) and is present in the dendritic branches and spines of DIV12-13 hippocampal neurons (see the EGFP signal in Fig. 1 B and Fig. S1 A). To compare the extent of reporter phosphorylation in spines, ratiometric images were created by normalizing the a-pS294 to EGFP signal intensities (Fig. 1 B and Fig. S1 A, ratio images). Only mushroom spines with clearly enlarged heads were chosen for the analysis. To confirm the specificity of the pS294 antibody signal, a mutant reporter construct containing alanine instead of the target serine was also investigated (S/A mutant). In all cases, S/A mutant reporter displayed only a negligible ratio signal (Fig. 1, B–D).

In untreated cells, phosphorylation of the PKD reporter was moderate and strongly increased by phorbol ester treatment (PDBu; Fig. 1, B and C). To inhibit endogenous PKD activity in neurons, which express all PKD isoforms, we applied the selective PKD inhibitor kbNB 142-70, which inhibits all three PKD isoforms at nanomolar concentrations and blocks PKD-mediated actions in vitro, whereas it is ineffective against other kinases in concentrations below 10 µM (LaValle et al., 2010a; Bravo-Altamirano et al., 2011; Ni et al., 2013). Application of 3 µM kbNB 142-70 significantly reduced the phosphorylation of the reporter compared with control cells (Fig. 1, B and C), indicating endogenous PKD activity within mushroom spines under basal conditions. Remarkably, kbNB 142-70 effectively inhibited PKD activity reporter phosphorylation in HEK293T cells and did not show toxic effects on embryonic cortical neuronal cultures in the applied concentration (Fig. S2, A–D).

Chemical treatments evoking different forms of plasticity activate PKD within dendritic spines

To investigate whether PKD-dependent mechanisms play a role in spine rearrangements, different chemical treatments were applied to hippocampal cultures. Glycine-induced chemical LTP (cLTP) is known to transiently activate NMDA receptors, leading to the strengthening of excitatory connections and spine enlargement within 1 h after stimulus (Lu et al., 2001; Goldin et al., 2001). In our hands, spine expansion occurred after 30 min and lasted for at least 2 h after cLTP induction (not depicted). Phosphorylation of the reporter in dendritic spines was strongly elevated at 5 min and sustained for at least 30 min after glycine treatment (Fig. 1, B and D).

Long-term depolarization leads to homeostatic regulation of structural and functional plasticity within neurons (Grubb and Burrone, 2010). Neurons were treated with 20 mM KCl, whereas 20 mM NaCl was added to the control cultures to compensate for osmotic changes. Excess KCl rapidly depolarized

the neurons (from −54.6 ± 0.9 mV resting potential [n = 27; mean ± SEM] to −28.8 ± 0.9 mV [n = 3]), silenced spontaneous neuronal activity, and prevented the formation of action potentials (Fig. S1 D), unless recorded neurons were hyperpolarized by injecting −200 pA negative current (Fig. S1 E). Despite this depolarization block, 16 h of KCl treatment did not affect the number of surviving neurons (Fig. S1 C). When KCl was washed out from the cultures, resting membrane potential rapidly returned to normal values (−49.7 ± 1 mV; n = 26) and neurons regained their normal activity, including the generation of single and burst-like spikes or receiving excitatory and inhibitory postsynaptic potentials (EPSPs and IPSPs, respectively; Fig. S1, F and G). Of note, 2 and 16 h of KCl treatment slightly increased cell viability in the cultures (Fig. S1 H).

KCl treatment activated PKD in the dendritic spines within 30 min, lasting for at least 2 h (Fig. 1, B and C) and with a uniform distribution along the axis of mushroom spines (Fig. S1, A and B). This effect was also evident at the culture level, as depolarization induced a long-lasting autophosphorylation of PKD on Ser910 (Fig. 2 C).

The PKD-specific inhibitor kbNB 142-70 blocked chemically induced reporter phosphorylation in both plasticity models (Fig. 1, B–D). Both MK-801 and APV, a noncompetitive and a competitive antagonist of NMDA receptors, respectively, reduced chemically induced reporter phosphorylation significantly (Fig. 1, B–D). It was reported that depolarization-induced homeostatic plasticity is regulated by the activation of L-type voltage-gated Ca^{2+} channels (Grubb and Burrone, 2010; Evans et al., 2013). In accordance, blocking L-type Ca^{2+} channels by 1 µM nifedipine completely prevented KCl-induced PKD reporter phosphorylation, whereas ω-conotoxin MVIIC (blocking N-, P-, and Q-type Ca^{2+} channels) proved to be ineffective (Fig. 1 C). Thus, our data indicate that elevated intracellular Ca^{2+} signal plays a role in the activation of PKD-dependent signaling pathways within dendritic spines.

Actin turnover within dendritic spines occurs in a biphasic manner during chemically induced plasticity

During structural and functional plasticity, the actin cytoskeleton rapidly reorganizes to allow the elaboration of the F-actin network, leading to the expansion of the spine head during LTP (Bosch et al., 2014). These events depend greatly on ADF/cofilin's actin-severing activity, increasing barbed ends of actin filaments, and providing the basis for the formation of a more complex network (Mizuno, 2013).

Cofilin activity is inhibited by its phosphorylation on Ser3, which is governed by LIMK1/2 and TESK, whereas dephosphorylation by the slingshot (SSH) phosphatase family activates cofilin (Mizuno, 2013). For cLTP treatment, overall p-cofilin level within the cultures increased significantly only after 120 min of glycine treatment. (Fig. 2 A). Interestingly, in parallel with an increase in pS910 autophosphorylation of PKD (Fig. 2 C), p-cofilin level was transiently reduced within the neuronal cultures during the initial 16 h of KCl application (Fig. 2 B).

To analyze cofilin phosphorylation and actin polymerization specifically within dendritic spines, we identified spine heads by PSD95 immunostaining and quantified the intensity of phosphorylated cofilin signal (Fig. 2, D–F), as well as actin-rhodamine incorporation within PSD95-positive dendritic spines (Fig. 2, G–I). Both cLTP and depolarization changed Ser3 phosphorylation of cofilin in a biphasic manner (Fig. 2, D–F). Relative p-cofilin intensity was reduced within PSD95-positive dendritic spine heads at 30 min and 2 h of cLTP or KCl treatment, respectively (Fig. 2, E and F). As compared with the Western blot data, these results more specifically indicate that cofilin is active within dendritic spines at these time points. At later stages, however, p-cofilin signal significantly increased within investigated spines (Fig. 2, E and F; 120 min and 16 h of cLTP and KCl treatment, respectively). At the same time, the actin barbed end assay indicated a significant decrease in actin incorporation within dendritic spines in KCl-induced depolarization compared with control cells (Fig. 2, H and I).

16 h of KCl-induced depolarization significantly increased the ratio of mushroom spines (Fig. 3, A and C) without affecting spine density (not depicted). KCl-induced changes in spine morphology were also evident when individual spines were plotted according to their length and HN index (head/neck width ratio; Fig. 3 B). As this happened at the expense of thin, filamentous spines, we assume that long-term depolarization leads to F-actin stabilization and, consequently, the expansion of dendritic spine heads. Collectively, our data indicate decreased actin dynamics when enlarged dendritic spine heads are already stabilized.

Depolarization modulates PKD pathways regulating actin turnover in vitro

PKD can increase cofilin phosphorylation by inhibition of SSH1 (Ser978) and activation of the PAK4 (Ser474)-LIMK1 pathway (see Olayioye et al. (2013) as a review). Thus, increased PKD activity shifts the balance toward inactive cofilin, leading to decreased actin binding and the inhibition of its actin-severing activity, thereby slowing down depolymerization and stabilizing the F-actin pool. Accordingly, specific inhibition of endogenous PKD activity by kbNB 142-70 decreased p-cofilin immunostaining (Fig. 2, E and F) and enhanced actin turnover within dendritic spines as revealed by the barbed end assay (Fig. 2, G and H). Importantly, kbNB 142-70 effectively blocked plasticity-induced F-actin stabilization in both chemical plasticity models, indicating that elevated PKD activity was required to sustain spine enlargement.

To assess the relation between PKD activity and the phosphorylation level of its substrates, we analyzed pPAK4 and pSSH1 signals upon KCl treatment. As the available antibodies were not suitable for the immunostaining of dendritic spines, we performed Western blot analyses without and with PKD inhibition (Fig. S2, E and H). Application of kbNB 142-70 reduced relative PAK4 and SSH1 phosphorylation compared with signal intensities obtained from time-matched DMSO-only treated samples, supporting that they are indeed downstream targets of PKD in neuronal cultures (Fig. S2, E–H).

Depolarization-dependent morphological changes in dendritic spines require PKD activity

Long-term application of kbNB 142-70 in control cultures slightly but not significantly decreased the ratio of mushroom spines in EGFP-transfected neurons (Fig. 3, A–C), without dramatically affecting morphological parameters of individual spines (Fig. 3 B). When kbNB 142-70 was applied to 16-h KCl-induced cultures, pharmacological inhibition of PKD prevented the enlargement of spine heads and the morphological transformation from filamentous to mushroom spines (Fig. 3, A and C).

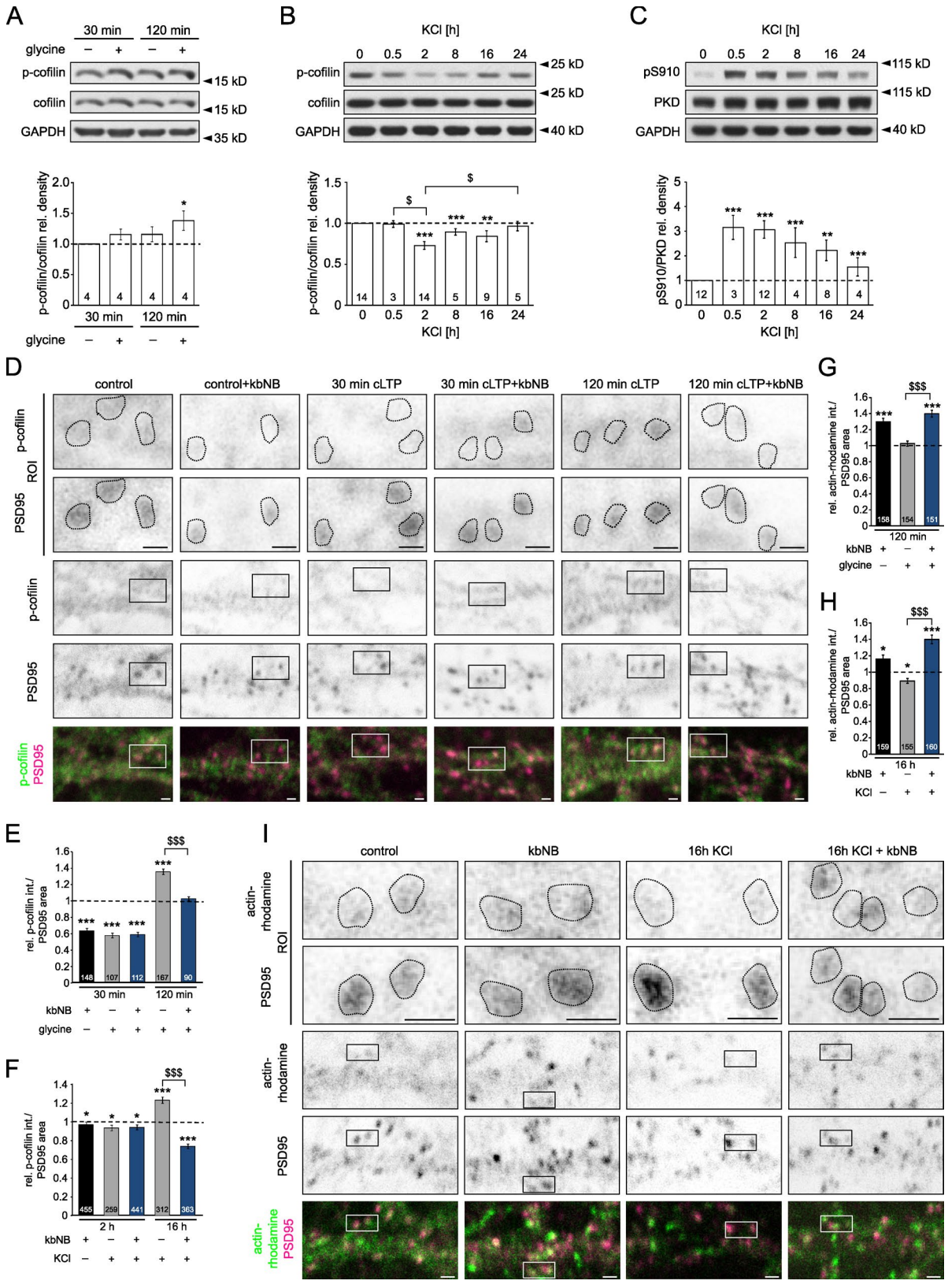

Figure 2. **Actin dynamics during chemically induced plasticity is regulated in a PKD-dependent manner.** (A and B) Relative changes in the Ser3 phosphorylation of cofilin during glycine-induced cLTP (A) or KCl-induced depolarization (B). (C) Temporal pattern of Ser910 phosphorylation of PKD during KCl-induced depolarization. Representative Western blots are displayed at the top. Graphs were calculated from 3–14 independent samples by normalizing phospho-specific/total protein/GAPDH ratios at the given time points to the nontreated values. (D) Inverted fluorescent and colored merged images of p-cofilin staining within PSD95-positive dendritic spines during cLTP treatment. The top rows show enlarged ROIs from the corresponding boxed areas in the lower-magnification images below. (E and F) Relative p-cofilin intensity values were normalized to the PSD area in cLTP (E)- or KCl (F)-treated cultures at the indicated time points. (G and H) Incorporation of actin-rhodamine during the stabilization of dendritic spines in cLTP (G)- or KCl (H)-treated

Mutation in the ATP-binding cassette of PKD1 (PKD1^{K612W}) inactivates the kinase and exerts a dominant-negative effect on all three isoforms (Czöndör et al., 2009; Rémillard-Labrosse et al., 2009; Ellwanger and Hausser, 2013). In accordance with pharmacological inhibition, expression of the EGFP-tagged dominant-negative PKD mutant (kdPKD-EGFP) reduced protrusion density in the tertiary branches of transfected neurons (Fig. 3, A and D) and increased the frequency of elongated, filamentous protrusions, along with a reduction of mushroom-shaped structures (Fig. 3 E). Dominant-negative kdPKD altered the remaining mushroom-shaped protrusions by decreasing their length and HN index, while significantly increasing the length of the thin spines (Fig. 3, F and G; Mann–Whitney *U* test, $P < 0.01$ for both types of spines). Thus, PKD activity plays a detectable role in F-actin stabilization during the later phase of depolarization, needed for sustaining enlarged spine heads in vitro.

Dominant-negative mutant PKD localizes to postsynaptic sites of hippocampal CA1 and CA3 neurons

To assess neuron-specific functions of PKD in vivo, we used a transgenic TetOn mouse line, allowing inducible expression of the dominant-negative kdPKD-EGFP protein (Czöndör et al., 2009). For better readability, doxycycline (DOX)-treated CaMKIIα-rtTA2 × kdPKD-EGFP double transgenic mice are named kdPKD-EGFP–expressing mice, whereas single transgenic littermates treated with DOX are referred to as the control group (Fig. 4, and Fig. 5, and Fig. S3).

In the case of 4–15 wk of DOX treatment, anti-GFP signal was detected only in kdPKD-EGFP–expressing mice, within the CA1 and CA3 regions of the hippocampus (Fig. 4, A and B; and Fig. 4, F and G, respectively), whereas other parts of the neocortex were negative or only scarcely labeled (not depicted). To visualize the subcellular localization of kdPKD-EGFP in these labeled neurons, electron micrographs were recorded from the CA1 stratum radiatum (Fig. 4, C–E) and from the CA3 stratum lucidum (Fig. 4, H and I). Because of the mosaic activation of rtTA2 in CaMKIIα rtTA2 mice (Michalon et al., 2005), the expression pattern was not homogenous within the hippocampus, leaving some of the pyramidal neurons devoid of the mutant protein (see Fig. 4 C showing neighboring dendritic spines with and without the expression of kdPKD-EGFP).

Anti-GFP Ni-DAB immunoprecipitate was evident in the dendrites of pyramidal neurons (Fig. 4, A and F), as well as within dendritic spines (Fig. 4, C and H, black arrows). To more precisely localize the mutant protein within spines, pre-embedding anti-GFP immunogold immunohistochemistry was also performed (Fig. 4, D and E). Gold particles were found in the close vicinity of the plasma- and endomembranes (note a labeled putative spine apparatus in Fig. 4 D) and in the neighborhood of the postsynaptic density (PSD) area. These findings suggest that dominant-negative PKD mutant protein localizes at the postsynaptic regions of neurons and in the periphery of dendritic spines.

Inhibition of endogenous PKD activity leads to altered morphology and shrinkage of hippocampal dendritic spines in vivo

Next, we investigated how the inhibition of endogenous PKD activity affects in vivo morphology of dendritic spines in control and kdPKD-EGFP–expressing animals treated with DOX for 10–12 wk (Fig. 4, J–M). In control CA1 slices, long-term DOX treatment did not affect dendritic spine morphology and architecture as the strong correlation between spine area and PSD length (Pearson correlation coefficient $r = 0.72$) was highly similar to the linear correlation obtained from wild-type CA1 spines (Hazai et al., 2013). However, kdPKD-EGFP–expressing CA1 spines were significantly smaller (Fig. 4 L) and had shorter PSD in comparison with their total area (Pearson correlation coefficient significantly reduced to $r = 0.38$; $P < 0.001$; Fig. 4 J).

Mossy fibers (MFs) originating from the granule cells of the dentate gyrus formed giant, multiple synapses on the dendritic spines of CA3 pyramidal neurons in the stratum lucidum (Fig. 4, H and I). Although the correlation between the area and PSD length values was not significantly changed (Pearson coefficient was 0.48 and 0.43 for control and kdPKD-EGFP spines, respectively), spine area and PSD length were significantly reduced by kdPKD-EGFP expression (Fig. 4, K and M). Additionally, kdPKD-EGFP–expressing spines possessed a more elongated morphology, leading to a significantly reduced circularity index. Collectively, our data emphasize that the inhibition of endogenous PKD activity modifies spine morphology both in vivo and in vitro.

Expression of kdPKD-EGFP in the hippocampus leads to the selective impairment of hippocampus-dependent learning abilities

Smaller dendritic spines normally confer reduced synaptic transmission, which may influence network activity. Therefore, we compared the activity of control and kdPKD-EGFP–expressing animals in different behavioral tests. After 5 wk of DOX treatment, neither spatial preference and overall motor performance nor explorative behavior differed in the open field experiments (Fig. 5, A and B; and Fig. S3, A–E).

Novelty-recognizing learning abilities were tested by the novel object recognition test before the onset (0 wk) and during the 12th week of DOX treatment (Fig. 5 C). The discrimination index (DI) was calculated by comparing the time spent with the new object relative to the familiar object after a 5-h retention interval. Control and kdPKD-EGFP–expressing animals spent more time exploring the novel object, regardless of the duration of the DOX treatment. As the DI was not changed by long-term DOX treatment in either group of animals, we can rule out deteriorative changes in the animals induced by DOX itself.

Hippocampus-related spatial learning abilities were compared by the Morris water maze and the radial maze tests after 9 or 15 wk of DOX treatment, respectively. In the water maze test, control and kdPKD-EGFP–expressing animals swam with the same mean speed during probe trials (Fig. S3 F). Between

cultures. (I) Inverted fluorescent and colored merged images of actin-rhodamine incorporation within PSD95-positive dendritic spines during KCl treatment. The top rows show enlarged ROIs from the corresponding boxed areas in the lower-magnification images below. (D and I) Bars, 1 µm. All data are displayed as mean ± SEM, and numbers of analyzed samples are indicated within the graphs. Dashed lines within graphs indicate control values. Asterisks represent significance compared with control values, and the $ symbol indicates significant differences between data pairs. * or $, $P < 0.05$; **, $P < 0.01$; *** or $$$, $P < 0.001$.

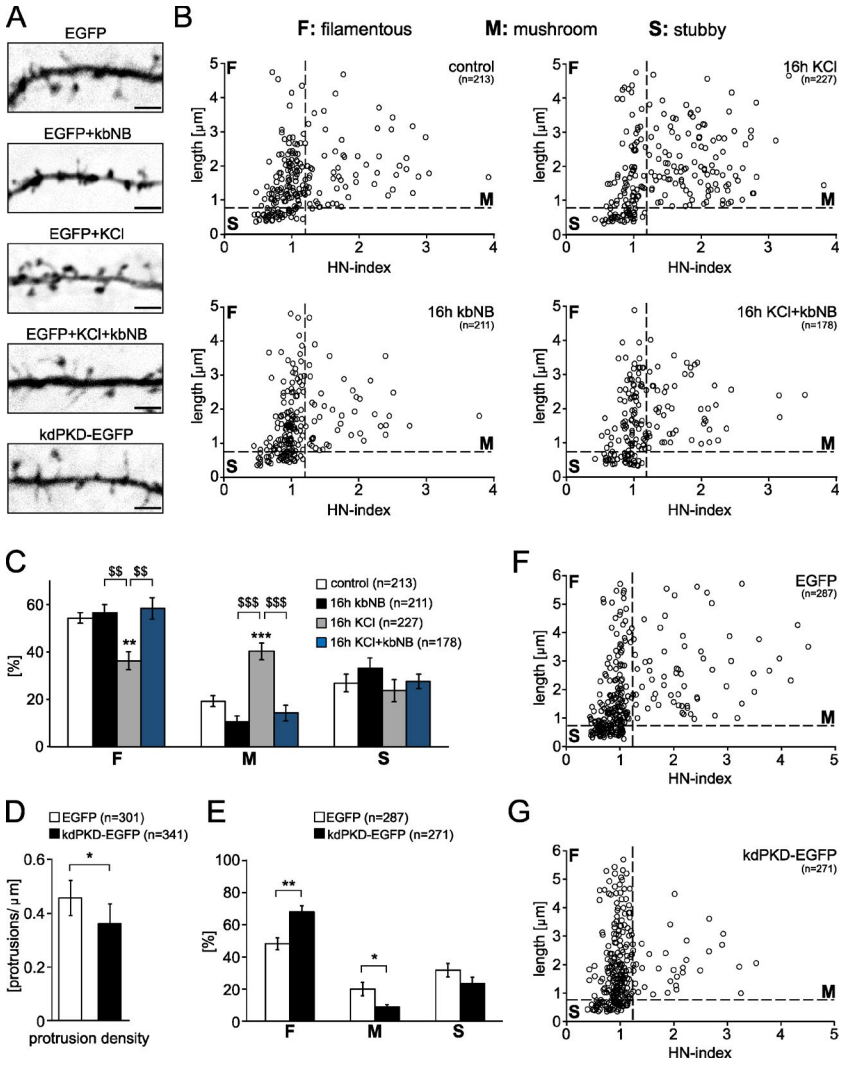

Figure 3. **PKD activity regulates spine morphology in cultured neurons.** (A) Representative inverted fluorescent images of tertiary dendritic branches of EGFP-transfected neurons treated with 20 mM KCl and/or 3 µM kbNB 142-70 or transfected with kdPKD-EGFP. Bars, 2 µm. (B and C) Morphological characteristics of dendritic spines in EGFP-transfected neurons, plotted along their head/neck width ratio (HN index) and length (B) and mean proportion of filamentous, mushroom, or stubby spines upon 16 h of 20 mM KCl and/or 3 µM kbNB 142-70 treatments (C). (D) Mean protrusion density on the tertiary branches of EGFP or kdPKD-EGFP–expressing neurons. (E) Mean proportion of filamentous, mushroom, or stubby spines in neurons transfected with EGFP or kdPKD-EGFP. (F and G) Morphological characteristics of dendritic spines in EGFP (F)- or kdPKD-EGFP (G)–transfected neurons, plotted along their head/neck width ratio (HN index) and length. Data were obtained from three to four independent cultures; the number of spines is indicated in the legends. All data are displayed as mean ± SEM. Asterisks represent significance compared with control values (white columns), and the $ symbol indicates significant differences between data pairs. *, $P < 0.05$; ** or \$\$, $P < 0.01$; *** or \$\$\$, $P < 0.001$.

the first (day 5) and second probe trials (day 10), control mice increased their searching activity for the removed platform as indicated by the elevated swim path and time spent over the target area (Fig. 5 E and Fig. S3 G). In contrast, kdPKD-EGFP–expressing mice performed significantly worse than controls on both days and were unable to improve their spatial memory even after 10 d of training. Fig. 5 D shows representative trajectories during the second probe trial.

In the eight-arm radial maze, the distance and time needed to find the baits positioned in every second arm were measured (Fig. 5 F and Fig. S3, H–L). The time spent in the center as well as in the baited and empty arms (Fig. S3, I and J), together with the number of entries into the baited or empty arms (Fig. S3, K and L), were also determined. Mean speed of control and kdPKD-EGFP mice was similar throughout the trials (12.4 ± 0.55 and 11.5 ± 0.77 cm/s, respectively). Animals performed similarly during the first week of the radial maze test. However, kdPKD-EGFP expression in the hippocampus prevented spatial learning during the second week of training. From the ninth day on, control animals ran significantly less and needed less time to find all four baits (Dunnett's post-hoc analysis, $P < 0.01$), whereas kdPKD-EGFP mice did not improve performance during the training sessions (Dunnett's post-hoc analysis, $P > 0.82$). Furthermore, kdPKD-EGFP–expressing mice spent significantly more time in the nonbaited arms and in the center compared with the control group (Fig. S3, I and J). In parallel, the number of entries into the empty (nonbaited) arms was also significantly higher (Fig. S3, K and L). These findings imply that hippocampus-related spatial memory is impaired upon long-term expression of kdPKD-EGFP in the hippocampus.

Hippocampal LTP formation is reduced by kdPKD-EGFP expression

To provide a mechanistic explanation for the observed deficits in hippocampus-related learning tasks, electrophysiological recordings were performed on acute hippocampal slices of control and kdPKD-EGFP–expressing mice after 10 to 14 wk of DOX treatment. Field potential was recorded from the stratum pyramidale of the CA1 area by either stimulating Schaffer collaterals (SCs) or MFs (Fig. 5, G–L). The mean amplitude of population spikes (POPSs) was significantly higher in the case of SC stimulation compared with MF stimulation in both groups of animals (Fig. 5 G), which is explained by the direct, monosynaptic stimulation of CA1 neurons via SC inputs. When single SC or MF stimuli were applied, no differences were found in the general excitability of control or kdPKD-EGFP–expressing slices (Fig. 5 G). Accordingly, E/S curves displaying the ratio between the slope of the EPSP (dEPSP) and the POPS amplitude (Wheal et al., 1998) were similar before tetanization (Fig. 5 K).

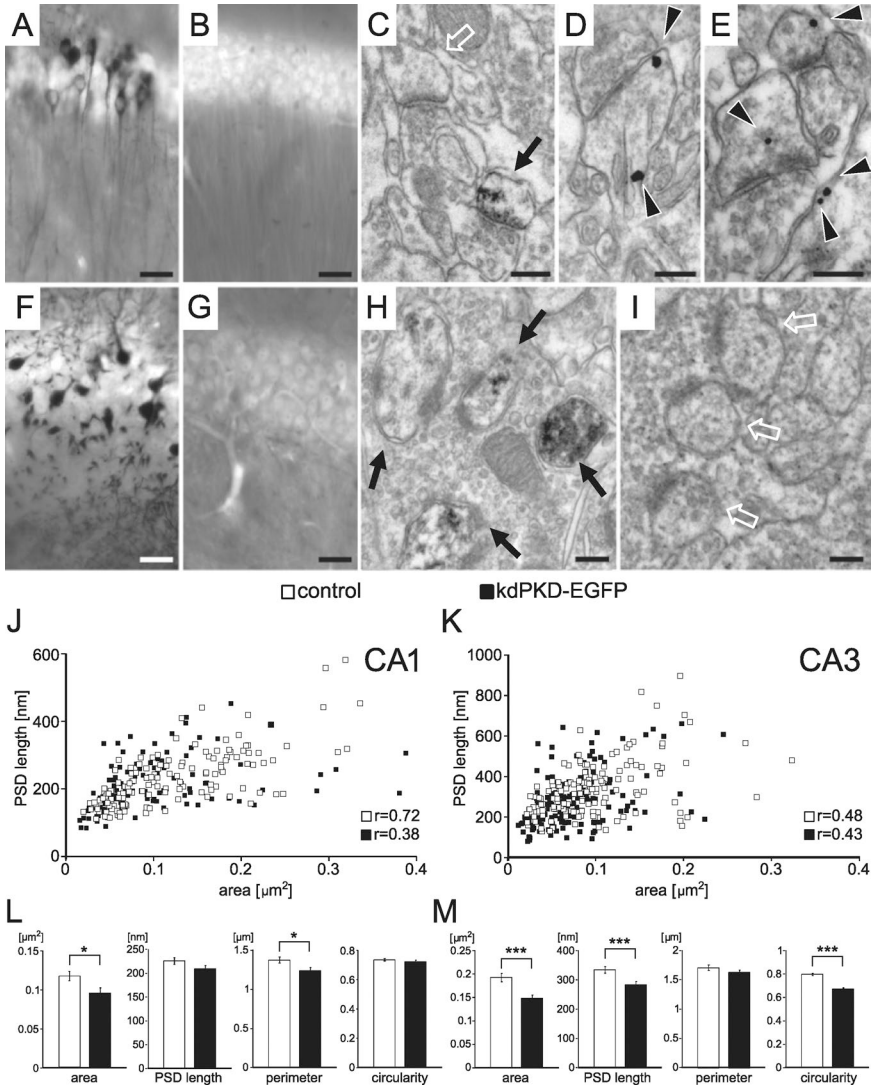

Figure 4. **Expression of the dominant-negative kdPKD-EGFP mutant in double transgenic hippocampal neurons alters dendritic spine morphology in vivo.** (A–I) α-EGFP staining in hippocampal CA1 (A–E) and CA3 (F–I) pyramidal neurons from kdPKD-EGFP–expressing (A, C–F, and H) or control mice (B, G, and I). (A, B, F, and G) Light microscopic DAB immunohistochemistry. (C, H, and I) Black arrows point to α-EGFP DAB precipitates in the dendritic spines of CA1 and CA3 dendrites, respectively. Nonlabeled spines are also present in the sections of kdPKD-EGFP mutant mice (white arrows in C and I). (D and E) Electron micrographs showing pre-embedded immunogold anti-GFP labeling (arrowheads) in the CA1 region. Bars: (A, B, F, and G) 30 µm; (C–E, H, and I) 200 nm. (J–M) Quantitative evaluation of the dendritic spines in the CA1 (J and L; 144 control and 114 kdPKD-EGFP spines) and CA3 (K and M; 142 control and 153 kdPKD-EGFP spines) regions of control and kdPKD-EGFP–expressing hippocampus. Pearson correlation values between spine profile area and PSD length are indicated in J and K. Graphs represent mean ± SEM. *, $P < 0.05$; ***, $P < 0.001$.

When high-frequency stimulation (HFS) was applied to the SCs, relative POPS amplitudes were enhanced in all cases, indicating the formation of LTP. However, 100-Hz tetanization in kdPKD-EGFP–expressing slices led to significantly reduced LTP compared with control slices (Fig. 5 I). For control slices, HFS induced robust facilitation as POPS amplitudes were larger for smaller dEPSP values. In contrast, facilitation was not detected when kdPKD-EGFP was expressed (Fig. 5 L). LTP in CA1 neurons was efficiently induced via a disynaptic transmission by the HFS of MFs, too, whereas kdPKD-EGFP–expressing neurons displayed a significantly impaired LTP compared with control slices (Fig. 5 J). These results are in line with the observed learning disabilities of kdPKD-EGFP–expressing mice and indicate that the lack of normal PKD functions within the CA1 and CA3 dendritic spines impairs synaptic plasticity.

Discussion

Although PKD has a well-established role in the regulation of the actin cytoskeleton and, consequently, cell migration or tumor metastasis in nonneuronal cells (see LaValle et al. (2010b) and Olayioye et al. (2013) as recent reviews), to our knowledge, our work is the first to address PKD-mediated effects on F-actin organization within dendritic spines. Our in vitro models show that activity-induced plasticity of dendritic spines depends on proper PKD functions. PKD activity increases during chemically induced cellular plasticity in cultured neurons and is required for stabilizing the F-actin network within enlarged dendritic spines. Consequently, inhibition of PKD activity, either by a specific PKD inhibitor or by expression of a dominant-negative PKD mutant, blocks activity-dependent changes in hippocampal dendritic spines, including morphological alterations as well as LTP formation, with an impact on spatial memory formation. Thus, PKD activity regulates synaptic plasticity in spines by regulating actin turnover and stability.

Chemically induced dendritic spine rearrangements proceed through a biphasic change in actin dynamics and require PKD activity

To test the importance of endogenous PKD activity within dendritic spines, we applied chemical stimulations known to induce different forms of plasticity. On one hand, glycine-induced cLTP is a method to stimulate specifically NMDA receptors only at synapses receiving spontaneous release of glutamate; thus, it closely mimics stimulus-induced synaptic potentiation, leading to the fast redistribution of the F-actin

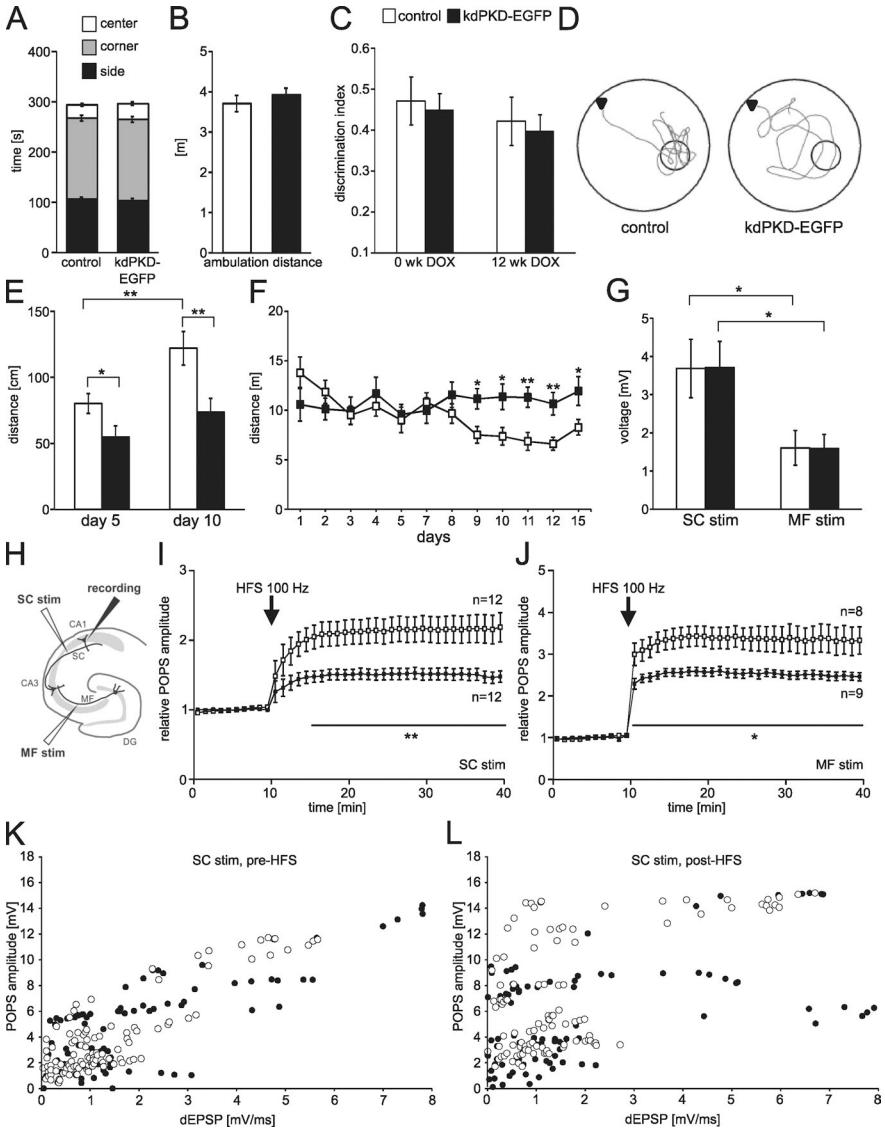

Figure 5. **Inhibition of endogenous PKD activity in hippocampal pyramidal neurons selectively impairs spatial memory formation and reduces LTP in CA1 hippocampal neurons.** Control (n = 16) and kdPKD-EGFP–expressing (n = 16) data are displayed by open and closed symbols and columns, respectively (B, C, and E–L). (A and B) Duration of time spent (A) and total running distance (B) within the open field. (C) Animals performed novel object recognition tests similarly before and during 12 wk of DOX. (D) Representative trajectories from control and kdPKD-EGFP–expressing mice during the second probe trial of the Morris water maze. Black triangles indicate start positions; the inner circles represent the target area over the original platform. (E) Distance swam within the target area during the first (day 5) and second (day 10) probe trials. (F) Mean distance needed to find all baits in the radial maze during the teaching process. (G) Mean POPS amplitudes evoked by single stimuli via SCs (SC stim) or MFs (MF stim). (H) Stimulation paradigm during LTP induction. (I and J) Relative POPS amplitudes after a 100-Hz HFS of the SCs (SC stim; I) or MFs (MF stim; J). (K and L) E/S curves describing POPS amplitudes in relation to the slope of the extracellular postsynaptic excitatory responses (dEPSP) determined in CA1 neurons before (K) or after (L) tetanization of the SCs. All data are shown as mean ± SEM. *, P < 0.05; **, P < 0.01.

network within dendritic spines (Lu et al., 2001; Goldin et al., 2001). On the other hand, prolonged depolarization of excitatory neurons induced by elevated extracellular KCl is known to induce long-term homeostatic changes, e.g., by increasing firing threshold via the distal relocation of the axon initial segment (Grubb and Burrone, 2010; Evans et al., 2013). In our hands, KCl induced a prolonged but reversible depolarization block and, as another morphological indicator of homeostatic plasticity, led to spine expansion within 16 h. Although axon initial segment relocation and spine enlargement are structurally different events, they seem to be regulated by L-type voltage-gated Ca^{2+} channels. The NMDA receptor–dependent activation of PKD, as demonstrated in both cLTP- and KCl-treated cultures, further indicates that elevated intracellular Ca^{2+} levels lead to PKD activation.

Under normal conditions, PKD has a basal activity leading to a slight decrease in actin turnover within the dendritic spines as p-cofilin intensity was reduced, whereas actin incorporation was elevated upon the application of kbNB 142-70. In contrast, endogenous PKD activity is not a key regulator of basal actin turnover in spines, as its inactivation has only mild effects on spine morphology.

LTP induced by high-frequency electrical as well as by chemical stimulation leads to enlargement of spine heads and/or increased ratio of mushroom spines and results in higher synaptic efficacy (Yuste, 2010). Stimulus-evoked structural and functional plasticity of dendritic spines during LTP evolves in a dynamic temporal manner: rapid reorganization of the spine actin cytoskeleton is followed by the stabilization of newly remodeled F-actin and delayed PSD enlargement (Bosch et al., 2014). Depending on the type of stimulus and the detection method, the timescale of these events can differ (Honkura et al., 2008; Rex et al., 2009; Bosch et al., 2014). Regardless of the chemical treatments used, PKD activation was evident during the early phase of spine rearrangements, when the actin pool was in a dynamic state as well as during later phases, paralleled by F-actin stabilization within the spines. Importantly, blocking of endogenous PKD functions efficiently prevented morphological enlargement of spines.

PKD regulates actin stabilization within dendritic spines

Expansion of dendritic spines during LTP requires the formation of a new stable population of actin at the core of the spine head, whereas increased F-actin polymerization continues below the

plasma membrane to generate the force required for spine enlargement (Bosch and Hayashi, 2012). Actin-binding proteins regulating F-actin treadmilling or network superstructure also show regional distribution within dendritic spines (Rácz and Weinberg, 2013). For example, cofilin is located within the dynamic shell region, near the plasma membrane (Racz and Weinberg, 2006). Intriguingly, immunogold detection of kdPKD-EGFP within hippocampal dendritic spines revealed a very similar localization of the mutant protein within the dynamic shell zone, in the close vicinity of the extrasynaptic plasma membrane. Thus, both regulatory players of the dynamic actin pool are located within the same subspine compartment.

As discussed in the previous section, chemically induced enlargement of dendritic spine heads goes through a transient, dynamic phase, when cofilin is activated and actin incorporation is elevated. Despite elevated PKD activity detected by increased autophosphorylation and by the PKD reporter, PKD inhibition did not detectably affect p-cofilin level in addition to that induced by the chemical stimulations themselves. Therefore, it is likely that PKD activity is counterbalanced by other pathways during this initial, dynamic phase that strongly shifts the cofilin cycle toward activation. Activation of NMDA receptors, for example, regulates the protein phosphatase 2B or calcineurin (Quinlan and Halpain, 1996), known to counterbalance phosphorylation of SSH1 (Wang et al., 2005). Additionally, PKD inhibition may affect other substrates known to regulate actin remodeling, e.g., cortactin (Eiseler et al., 2010), too. Cortactin is concentrated in dendritic spines of cultured hippocampal neurons and has been implicated in the activity-dependent regulation of spine morphogenesis as well (Hering and Sheng, 2003).

Inactivation of cofilin by Ser3 phosphorylation occurs during LTP and leads to an increase in F-actin levels as well as to the appearance of enlarged spine heads (Fukazawa et al., 2003; Chen et al., 2007). During the consolidating phase of spine rearrangements, PKD activity was required for morphological rearrangements as well as for cofilin inactivation and actin stabilization. Although a kbNB 142-70–mediated decrease in PAK4 and SSH1 phosphorylation was detectable in the cultures only up to 8 h of depolarization, this could be the result of the insensitivity of Western blot to detect subcellular and tissue-specific phosphorylation events at later time points. Nevertheless, our data provide convincing evidence that PKD-mediated regulation of F-actin stabilization is needed especially during the consolidating, late phase of plasticity-induced spine enlargement.

PKD regulates synaptic plasticity and memory formation

According to pre-HFS data, kdPKD-EGFP expression did not influence basal synaptic activity, which is concordant with the similar performance during the initial training days in spatial learning tests. Thus, compensatory mechanisms within the neuronal circuitry act in a homeostatic way to preserve baseline synaptic activity even when endogenous PKD activity is impaired (Mateos et al., 2007; Segal, 2010). In contrast, HFS revealed important differences between control and kdPKD-EGFP–expressing mice. Although E/S potentiation (Wheal et al., 1998) was evident in control recordings, it was inhibited upon kdPKD-EGFP expression. As the increase in POPS amplitudes upon HFS was reduced in kdPKD-EGFP recordings, we conclude that postsynaptic inhibition of endogenous PKD functions is responsible for decreased LTP. This is in accordance with the localization of the mutant PKD protein within the dendritic spines and dendrites of CA1 neurons.

So far, PKD has been indicated in a special form of associative learning observed in *Caenorhabditis elegans*: DKF-2B, a neuron-specific PKD isoform of the worm, is essential for the starvation-induced avoidance of previously attractant salt taste (Fu et al., 2009) and, recently, in cocaine-induced locomotor hyperactivity (Wang et al., 2014). In our experiments, ablation of endogenous PKD activity within the hippocampus specifically inhibited spatial learning without affecting motor coordination, overall anxiety, or object recognition performance, which are regulated by hippocampus-independent circuits (Antunes and Biala, 2012). In the Morris water maze and the radial maze, which are widely used to test hippocampus-dependent spatial memory formation (Sharma et al., 2010), kdPKD-EGFP animals showed no improvement. Although reentry into the originally baited arms (representing working memory error) was similar in comparison with controls, kdPKD-EGFP animals frequently entered into never-baited arms, which is an additional sign of impaired spatial reference memory (Sharma et al., 2010). Importantly, cofilin-dependent actin dynamics are specifically required for associative learning, whereas short-term working memory and exploratory learning are cofilin independent (Rust et al., 2010).

Morphological changes as well as plasticity within dendritic spines are dependent on several molecular factors. In neurons, PKD so far regulates intracellular transport, surface localization, and phosphorylation of transmembrane receptors (Cabrera-Poch et al., 2004; Bisbal et al., 2008; Wang et al., 2014; Quassollo et al., 2015), development and maintenance of dendritic arborization (Horton et al., 2005; Czöndör et al., 2009), production of growth factors (Xu et al., 2013), and neurotrophin signaling (Arévalo et al., 2006). Besides all of these possible effects, our work provides evidence that during activity-induced potentiation and enlargement of spines, PKD is a major regulator of F-actin stabilization, directly influencing learning and memory formation.

Materials and methods

Animal handling

CD1, CaMKIIα-rtTA2 (Michalon et al., 2005), or kdPKD1-EGFP (Czöndör et al., 2009) transgenic mice were housed in the animal facility at 22 ± 1°C, with 12-h light/dark cycles and ad libitum access to food and water. All experiments complied with local guidelines and regulations for the use of experimental animals (PEI/001/1108-4/2013 and PEI/001/1109-4/2013 for the experiments performed in Budapest), in agreement with the European Union and Hungarian legislation, or were approved by the Regierungspräsidium Stuttgart. DOX was administered in wet food at 6-mg/g dose for up to 16 wk with ad libitum access.

Cell cultures, transfection, and chemical treatment

Primary cultures of embryonic hippocampal cells were prepared from CD1 mice on embryonic day 17–18 according to Czöndör et al. (2009). Cells were seeded onto poly-L-lysine–laminin (Sigma-Aldrich)-coated glass coverslips in 24-well plates at 1.5×10^5 cells/well or onto poly-L-lysine–coated 6-well plates at 7×10^5 or 96-well plates at 3×10^4 cells/well density. Cells were transfected using Lipofectamine 2000 (Invitrogen) with the following constructs: PKDreporter-pEGFP-C1-L-pS294-L, PKDreporter-pEGFP-C1-L-pS294A-L (Czöndör et al., 2009), pEGFP-N1 (Takara Bio Inc.), and pEGFP-N1-PKCμ^{K612W} (Hausser et al., 2002). Cultures were treated with 1 μM phorbol 12,13-dibutyrate (PDBu; Sigma-Aldrich), 1 μM nifedipine (Sigma-Aldrich), and 3 μM kbNB 142-70,

10 µM MK-801, 50 µM APV, or 1 µM ω-conotoxin MVIIC (all from Tocris Bioscience) for the indicated time. Depolarization was induced by adding 20 mM KCl to the culture medium, reaching 25 mM KCl in total. In control cultures, 20 mM NaCl was applied.

cLTP was performed at 37°C. Cells were incubated in ECS buffer (150 mM NaCl, 2 mM $CaCl_2$, 5 mM KCl, 10 mM Hepes, 30 mM glucose, 0.5 µM tetrodotoxin, 20 µM bicuculline, and 1 µM strychnine, pH 7.4) for 5 min. 200 µM glycine was applied for 3 min in ECS buffer, and then medium was changed back to the original medium, in which cells survived for an additional 5, 30, or 120 min. Inhibitors (APV or kbNB 142-70) were present in the buffers throughout the experiment. Antagonists were all from Tocris Bioscience.

Whole cell patch clamp recordings

Electrophysiological recordings of hippocampal neurons were performed under an A1 AxioObserver microscope (Carl Zeiss). Spontaneous activity and evoked responses were recorded at room temperature (21–23°C) under whole cell conditions. Signals were amplified using a MultiClamp700B (Molecular Devices) and acquired at 20 kHz using the data acquisition software DASYLab version 11 (National Instruments). Patch pipettes were pulled from standard wall glass of 1.5 mm OD (Warner Instruments) and had input resistances of 7–10 MOhm. The composition of the bath solution (aCSF) was (mM) 125 NaCl, 3.5 KCl, 2 $CaCl_2$, 1.2 $MgCl_2$, 1.25 NaH_2PO_4, 25 $NaHCO_3$, and 10 glucose, pH 7.4. For depolarizing treatment, an additional 20 mM KCl or NaCl was added. For recording action potentials and voltage-gated currents, patch electrodes were filled with the following solution (mM): 100 K-Gluconate, 10 KCl, 10 KOH, 10 Hepes, and 0.2 EGTA, pH 7.3. To record voltage responses of the neurons, stepwise current commands of 350-ms duration were used, starting at −200 pA and incremented by 5 pA. Analysis of the evoked responses was performed by software developed by A. Szűcs (IVAnalyzer). Multiple physiological parameters, including the resting membrane potential, rheobase, input resistance at rest, spike amplitude, and half-width, among others, were determined for each cell.

Immunostaining and microscopy in fixed cultures

Cultures were fixed with 4% paraformaldehyde and immunostained essentially as described by Czöndör et al. (2009). Primary antibodies were a-pS294 (anti-PI4KIIIB-pS294, mouse, 1:1,000; Sigma-Aldrich), a–p-cofilin (pSer3, rabbit, 1:1,000; Cell Signaling Technology), and anti-PSD95 (mouse, 1:500; Thermo Fisher Scientific). Appropriate Alexa Fluor–labeled secondary antibodies (Invitrogen) were applied in 1:500 dilution. Images were taken with an LSM 710 (Carl Zeiss) or with a FluoView 500 LSM IX81 (Olympus) microscope with Plan Apochromat 63×/1.4 or Plan Apochromat 60×/1.1 immersion objectives, respectively, using 0.8–airy unit aperture. a-pS294/EGFP ratio images within dendritic spines were calculated using the Ratio Plus plugin of ImageJ (National Institutes of Health) by summarizing the intensity of three adjacent Z-stacks within the manually drawn regions of interest (ROIs), followed by subtracting background fluorescent intensity. a-pS294/EGFP ratio along the dendritic spines was determined along a 10-pixel-wide line drawn from the head to the shaft regions. For p-cofilin staining, single PSD95-positive spine heads were delineated manually in the appropriate Z-stack, and mean p-cofilin intensity was determined within these ROIs by ImageJ and normalized to the PSD area. In all parallel experiments, images were recorded with the same microscopic settings with 0.7–airy unit aperture. All experiments were repeated at least three times using independent cultures. Measurements and morphological characterization of dendritic protrusions were performed manually, using ImageJ according to the following criteria: stubby and filamentous spines possessed an HN index below 1.2, while they were either shorter or longer than 0.8 µm, respectively; mushroom spines had an HN index above 1.2, with a length exceeding 0.8 µm.

Actin barbed end assay

Actin barbed end assay was performed in barbed end buffer (138 mM KCl, 20 mM Hepes, 3 mM EGTA, 4 mM $MgCl_2$, and 1% BSA, pH 7.5) at 37°C. After a brief wash, cultures were treated with 0.45 µM rhodamine-conjugated nonmuscle G-actin (Cytoskeleton) for 2 min in barbed end buffer containing 0.2 mg/ml saponin, 1 mM ATP, and 0.5 mM DTT at 37°C. Cultures were fixed in 4% PFA in PHEM buffer (60 mM Pipes, 25 mM Hepes, 10 mM EGTA, 2 mM $MgCl_2$, and 0.12 M sucrose, pH 7.0) and stained for PSD95 (see previous section). Images were taken with a FluoView 500 IX81 microscope using a Plan Apochromat 60×/1.1 immersion objective with identical microscopic settings with 0.8–airy unit aperture. Mean rhodamine-actin intensity values were determined within ROIs manually drawn over PSD95-positive dendritic spines and normalized to the PSD area.

Western blot

Whole cell extracts from hippocampal neuronal cultures were obtained by harvesting in lysis buffer as described in Czöndör et al. (2009). Equal protein amounts of the corresponding samples were subjected to SDS-PAGE (NuPAGE Novex Bis-Tris Gel; 4–12%; Invitrogen) and blotted onto nitrocellulose membrane (Life Sciences). After blocking with 0.5% blocking reagent (Roche) in PBS–0.05% Tween, membranes were probed with specific antibodies as follows: anti–phospho-PKD (a-pS910 rabbit, 1:2,000; Hausser et al., 2002), anti-PKD1 (C20 rabbit, 1:2,000; Santa Cruz Biotechnology, Inc.), anti–p-cofilin (pSer3 rabbit, rabbit, 1:1,000; Cell Signaling Technology), anti-cofilin (rabbit, 1:1,000; Cell Signaling Technology), anti-phospho–Slingshot-1L (pSer978 rabbit, 1:1,000; ECM Biosciences), anti–Slingshot-1L (rabbit, 1:1,000; Abcam), anti–phospho-PAK4/5/6 (pSer474/602/560 rabbit, 1:2,000; Cell Signaling Technology), anti-PAK4 (rabbit, 1:1,000; Cell Signaling Technology), and anti-GAPDH (rabbit, 1:6,000; Sigma-Aldrich).

Signals were visualized with horseradish peroxidase–coupled secondary antibodies (1:10,000; Dianova) using ECL or the SuperSignal West Dura Luminol enhancer substrate. Membranes were stripped in 62.5 mM Tris, pH 6.8, 2% SDS, and 14.3 mM β-mercaptoethanol for 30 min at 50°C and then reprobed with the indicated antibodies. Mean intensity values were calculated from 2–13 independent cultures using ImageQuant TL software (GE Healthcare) as phospho-specific/total protein/GAPDH ratios. Relative inhibition of phosphorylation by kbNB 142-70 was determined by comparing mean intensity values between kbNB-treated and nontreated samples from the same time point. Normalized values from 3–14 independent cultures were averaged.

Cell viability and neuronal survival assays

Viability of the cultures treated with an excess of 20 mM KCl or NaCl was measured by the MTT assay. Cells grown in 96-well plates were treated with 3-(4,5-dimethylthiazol-2-yl)-2,5-diphenyltetrazolium bromide (MTT; Sigma-Aldrich) in a final concentration of 250 µg/ml for 40 min and then dissolved in acidic (0.08 M HCl) isopropanol (Merck). OD was determined at 570 nm with an ELISA reader (Bio-Rad Laboratories). Mean viability values were normalized to data obtained from nontreated cells. Neuronal survival was determined by calculating the percentage of neurons with distorted phase-contrast picture and pyknotic nuclei revealed by DAPI staining. At least 30 fields of view were analyzed from three independent cultures.

EM

Experiments were performed in 5–6-mo-old control and kdP-KD-EGFP–expressing animals, which were fed for 10–12 wk with

DOX. Aldehyde-fixed brain sections from perfused animals were processed by standard immunoperoxidase EM protocol (for details see Racz and Weinberg (2006)) using a polyclonal rabbit anti-GFP antibody (1:1,000; Invitrogen). Plastic-embedded ultrathin sections were examined in a T1011 electron microscope (JEOL) at 80 KV; images were collected with a MegaView (Soft Imaging System) 12-bit 1024 × 1024 charge-coupled device camera.

Electron micrographs of randomly selected fields containing immunolabeled pyramidal neurons were taken from the middle 1/3 region of CA1 stratum radiatum or CA3 stratum lucidum. Spine profiles were selected for quantitative analysis only when they contained a clear PSD and were opposed to presynaptic boutons containing synaptic vesicles. Synaptic profile areas, perimeters, and profile circularity ($4\pi \times \text{area}/\text{perimeter}^2$) were measured by ImageJ.

Behavioral tests

16 control (single transgene) and 16 double transgenic male littermates were used from kdPKD-EGFP$^{+/+}$ × CamKIIα rtTA2$^{+/-}$ breedings. DOX treatment was started from the 7th to 10th weeks of age and lasted for 16 wk altogether. Novel object recognition was performed before the onset and during the 12th week of treatment. Mice were habituated to the arena for 5 min. The next day, animals explored two identical objects for 5 min (A1 and A2) and then 5 h later one familiar (A1) and a novel (B) object again for 5 min. Object exploration time was defined as the time spent sniffing at the objects. The DI was calculated as (B exploration time − A1 exploration time)/(B exploration time + A1 exploration time). The open field test was executed in the fifth week of DOX treatment. Mice were placed in the middle of a 48 × 48 × 40-cm open arena (Experimetria Ltd.) and were allowed to move freely for 5 min. Their behavior and trajectories were monitored and analyzed by the Conducta Advanced System 1.0. Morris water maze tests were performed during the 9th and 10th weeks of DOX. A round, 105-cm diameter tank was filled with 25 cm of water (22 ± 1°C). On day 0, a visible platform was placed into the pool with visual cues on the walls. Mice were allowed to swim for a maximum 60 s. If they failed to reach the platform, they were placed on it for 20 s. From day 1, the escape platform (8-cm diameter) was submerged 1 cm below the surface of the water. Mice were trained for 10 consecutive days, with four trials per day. On the 5th and 10th day, the platform was removed, and the time and distance spent searching around a 24-cm diameter area over the original platform was calculated. The radial arm maze test was performed during the 15th to 16th week of DOX treatment, essentially as described by Gellért et al. (2012). Mice were habituated to the radial maze for four consecutive days, and then four baits were positioned into every second arm. During the task, mice were positioned at the center, and the time and trajectories needed for finding all baits were recorded.

Electrophysiological recording of hippocampal synaptic transmission

Experiments were performed essentially as described in Borbély et al. (2009). In short, mice were decapitated under ether anesthesia, and 400-µm-thick horizontal hippocampal slices were cut. Slices were stored at room temperature for 1 h in carbogenated (95% O_2 and 5% CO_2) standard artificial cerebrospinal fluid and then transferred into a Haas-type recording chamber with continuous artificial cerebrospinal fluid perfusion and carbogene saturation at 33 ± 1°C.

Glass microelectrodes filled with 1 M NaCl were positioned as recording electrodes in the stratum pyramidale of the hippocampal CA1 region, whereas bipolar tungsten-stimulating electrodes were positioned either at the MF tract to evoke disynaptic POPSs or at the SCs to evoke monosynaptic responses. Amplified and conditioned signal was digitized for subsequent off-line analysis.

The viability of slices was tested before each experiment. If POPS amplitude at maximum stimulus intensity was smaller than 3 mV, the slice was excluded from the experiments. Slices were tetanized with the intensity that elicited 70% of maximal POPS amplitude. At the beginning of the data recording session, 0.1-Hz continuous stimulation was applied for 10 min (test stimulation), and then HFS trains (2× 6-s 100-Hz stimulus train, 10-s interval) were applied for LTP induction. Subsequently, 0.1-Hz continuous test stimulation was used to detect the changes in excitability during 30 min. Averaged responses evoked at medium stimulation intensity were calculated as a mean of amplitude of six POPSs before and during the 30 min after LTP induction.

Statistical analyzes of the data

For statistical evaluation, Student's *t* test, Tukey's post-hoc, or nonparametric Mann–Whitney tests were used. Excel (Microsoft), Kaleidagraph (Synergy Software), or SPSS Statistics (IBM) was used to compute statistics. Data are displayed as mean ± SEM, unless otherwise indicated.

Online supplemental material

Fig. S1 shows depolarization-induced changes in PKD activity reporter phosphorylation, neuronal viability, and electrophysiological properties. Fig. S2 shows concentration-dependent effects of PKD inhibitors on the phosphorylation of PKD activity reporter and their toxicity and the relative inhibition of PKD-mediated phosphorylation of downstream targets by kbNB 142-70. Fig. S3 provides additional behavioral data from the open field, Morris water maze, and radial maze tests. Online supplemental material is available at http://www.jcb.org/cgi/content/full/jcb.201501114/DC1.

Acknowledgements

We are grateful to Krisztina Móritz, Judit Laszy, Marianna Ruszka, and Dániel Varga for their help in establishing the appropriate behavioral experiments and Tünde Magyar and Renáta Pop for the technical assistance of EM preparations.

Research was supported by Hungarian Scientific Research Foundation grants K81934 to K. Schlett and K83830 to B. Rácz, by the KTIA_NAP_13-2014-0018 to K. Schlett, by the 39957 MÖB-DAAD travel exchange program to K. Schlett and A. Hausser, by the PF247/13-1 DFG project to K. Pfizenmaier and K. Schlett, and by the Gedeon Richter Centenarium Foundation to N. Bencsik and K. Schlett. B. Rácz is supported by the Research Faculty Grant 2014 of the Faculty of Veterinary Science, Szent István University, and by the János Bolyai Research Fellowship of the Hungarian Academy of Sciences.

The authors declare no competing financial interests.

Submitted: 28 January 2015
Accepted: 23 July 2015

References

Antunes, M., and G. Biala. 2012. The novel object recognition memory: neurobiology, test procedure, and its modifications. *Cogn. Process.* 13:93–110. http://dx.doi.org/10.1007/s10339-011-0430-z

Arévalo, J.C., D.B. Pereira, H. Yano, K.K. Teng, and M.V. Chao. 2006. Identification of a switch in neurotrophin signaling by selective tyrosine phosphorylation. *J. Biol. Chem.* 281:1001–1007. http://dx.doi.org/10.1074/jbc.M504163200

Bisbal, M., C. Conde, M. Donoso, F. Bollati, J. Sesma, S. Quiroga, A. Díaz Añel, V. Malhotra, M.P. Marzolo, and A. Cáceres. 2008. Protein kinase D regulates trafficking of dendritic membrane proteins in devel-

oping neurons. *J. Neurosci.* 28:9297–9308. http://dx.doi.org/10.1523/JNEUROSCI.1879-08.2008

Borbély, S., E. Dobó, D. Czégé, E. Molnár, M. Bakos, B. Szucs, A. Vincze, I. Világi, and A. Mihály. 2009. Modification of ionotropic glutamate receptor-mediated processes in the rat hippocampus following repeated, brief seizures. *Neuroscience.* 159:358–368. http://dx.doi.org/10.1016/j.neuroscience.2008.12.027

Bosch, M., and Y. Hayashi. 2012. Structural plasticity of dendritic spines. *Curr. Opin. Neurobiol.* 22:383–388. http://dx.doi.org/10.1016/j.conb.2011.09.002

Bosch, M., J. Castro, T. Saneyoshi, H. Matsuno, M. Sur, and Y. Hayashi. 2014. Structural and molecular remodeling of dendritic spine substructures during long-term potentiation. *Neuron.* 82:444–459. http://dx.doi.org/10.1016/j.neuron.2014.03.021

Bravo-Altamirano, K., K.M. George, M.-C. Frantz, C.R. LaValle, M. Tandon, S. Leimgruber, E.R. Sharlow, J.S. Lazo, Q.J. Wang, and P. Wipf. 2011. Synthesis and structure-activity relationships of benzothienothiazepinone inhibitors of protein kinase D. *ACS Med Chem Lett.* 2:154–159. http://dx.doi.org/10.1021/ml100230n

Cabrera-Poch, N., L. Sánchez-Ruiloba, M. Rodríguez-Martínez, and T. Iglesias. 2004. Lipid raft disruption triggers protein kinase C and Src-dependent protein kinase D activation and Kidins220 phosphorylation in neuronal cells. *J. Biol. Chem.* 279:28592–28602. http://dx.doi.org/10.1074/jbc.M312242200

Chen, L.Y., C.S. Rex, M.S. Casale, C.M. Gall, and G. Lynch. 2007. Changes in synaptic morphology accompany actin signaling during LTP. *J. Neurosci.* 27:5363–5372. http://dx.doi.org/10.1523/JNEUROSCI.0164-07.2007

Czöndör, K., K. Ellwanger, Y.F. Fuchs, S. Lutz, M. Gulyás, I.M. Mansuy, A. Hausser, K. Pfizenmaier, and K. Schlett. 2009. Protein kinase D controls the integrity of Golgi apparatus and the maintenance of dendritic arborization in hippocampal neurons. *Mol. Biol. Cell.* 20:2108–2120. http://dx.doi.org/10.1091/mbc.E08-09-0957

Eiseler, T., A. Hausser, L. De Kimpe, J. Van Lint, and K. Pfizenmaier. 2010. Protein kinase D controls actin polymerization and cell motility through phosphorylation of cortactin. *J. Biol. Chem.* 285:18672–18683. http://dx.doi.org/10.1074/jbc.M109.093880

Ellwanger, K., and A. Hausser. 2013. Physiological functions of protein kinase D in vivo. *IUBMB Life.* 65:98–107. http://dx.doi.org/10.1002/iub.1116

Evans, M.D., R.P. Sammons, S. Lebron, A.S. Dumitrescu, T.B. Watkins, V.N. Uebele, J.J. Renger, and M.S. Grubb. 2013. Calcineurin signaling mediates activity-dependent relocation of the axon initial segment. *J. Neurosci.* 33:6950–6963. http://dx.doi.org/10.1523/JNEUROSCI.0277-13.2013

Frost, N.A., J.M. Kerr, H.E. Lu, and T.A. Blanpied. 2010. A network of networks: cytoskeletal control of compartmentalized function within dendritic spines. *Curr. Opin. Neurobiol.* 20:578–587. http://dx.doi.org/10.1016/j.conb.2010.06.009

Fu, Y., M. Ren, H. Feng, L. Chen, Z.F. Altun, and C.S. Rubin. 2009. Neuronal and intestinal protein kinase d isoforms mediate Na^+ (salt taste)–induced learning. *Sci. Signal.* 2:ra42. http://dx.doi.org/10.1126/scisignal.2000224

Fuchs, Y.F., S.A. Eisler, G. Link, O. Schlicker, G. Bunt, K. Pfizenmaier, and A. Hausser. 2009. A Golgi PKD activity reporter reveals a crucial role of PKD in nocodazole-induced Golgi dispersal. *Traffic.* 10:858–867. http://dx.doi.org/10.1111/j.1600-0854.2009.00918.x

Fukazawa, Y., Y. Saitoh, F. Ozawa, Y. Ohta, K. Mizuno, and K. Inokuchi. 2003. Hippocampal LTP is accompanied by enhanced F-actin content within the dendritic spine that is essential for late LTP maintenance in vivo. *Neuron.* 38:447–460. http://dx.doi.org/10.1016/S0896-6273(03)00206-X

Gellért, L., D. Varga, M. Ruszka, J. Toldi, T. Farkas, I. Szatmári, F. Fülöp, L. Vécsei, and Z. Kis. 2012. Behavioural studies with a newly developed neuroprotective KYNA-amide. *J. Neural Transm.* 119:165–172. http://dx.doi.org/10.1007/s00702-011-0692-8

Goldin, M., M. Segal, and E. Avignone. 2001. Functional plasticity triggers formation and pruning of dendritic spines in cultured hippocampal networks. *J. Neurosci.* 21:186–193.

Grubb, M.S., and J. Burrone. 2010. Activity-dependent relocation of the axon initial segment fine-tunes neuronal excitability. *Nature.* 465:1070–1074. http://dx.doi.org/10.1038/nature09160

Hausser, A., G. Link, L. Bamberg, A. Burzlaff, S. Lutz, K. Pfizenmaier, and F.-J. Johannes. 2002. Structural requirements for localization and activation of protein kinase C μ (PKCμ) at the Golgi compartment. *J. Cell Biol.* 156:65–74. http://dx.doi.org/10.1083/jcb.200110047

Hazai, D., R. Szudoczki, J. Ding, S.H. Soderling, R.J. Weinberg, P. Sótonyi, and B. Rácz. 2013. Ultrastructural abnormalities in CA1 hippocampus caused by deletion of the actin regulator WAVE-1. *PLoS ONE.* 8:e75248. http://dx.doi.org/10.1371/journal.pone.0075248

Hering, H., and M. Sheng. 2003. Activity-dependent redistribution and essential role of cortactin in dendritic spine morphogenesis. *J. Neurosci.* 23:11759–11769.

Holtmaat, A., and K. Svoboda. 2009. Experience-dependent structural synaptic plasticity in the mammalian brain. *Nat. Rev. Neurosci.* 10:647–658. http://dx.doi.org/10.1038/nrn2699

Honkura, N., M. Matsuzaki, J. Noguchi, G.C.R. Ellis-Davies, and H. Kasai. 2008. The subspine organization of actin fibers regulates the structure and plasticity of dendritic spines. *Neuron.* 57:719–729. http://dx.doi.org/10.1016/j.neuron.2008.01.013

Horton, A.C., B. Rácz, E.E. Monson, A.L. Lin, R.J. Weinberg, and M.D. Ehlers. 2005. Polarized secretory trafficking directs cargo for asymmetric dendrite growth and morphogenesis. *Neuron.* 48:757–771. http://dx.doi.org/10.1016/j.neuron.2005.11.005

LaValle, C.R., K. Bravo-Altamirano, K.V. Giridhar, J. Chen, E. Sharlow, J.S. Lazo, P. Wipf, and Q.J. Wang. 2010a. Novel protein kinase D inhibitors cause potent arrest in prostate cancer cell growth and motility. *BMC Chem. Biol.* 10:5. http://dx.doi.org/10.1186/1472-6769-10-5

LaValle, C.R., K.M. George, E.R. Sharlow, J.S. Lazo, P. Wipf, and Q.J. Wang. 2010b. Protein kinase D as a potential new target for cancer therapy. *Biochim. Biophys. Acta.* 1806:183–192.

Lu, W., H. Man, W. Ju, W.S. Trimble, J.F. MacDonald, and Y.T. Wang. 2001. Activation of synaptic NMDA receptors induces membrane insertion of new AMPA receptors and LTP in cultured hippocampal neurons. *Neuron.* 29:243–254. http://dx.doi.org/10.1016/S0896-6273(01)00194-5

Mateos, J.M., A. Lüthi, N. Savic, B. Stierli, P. Streit, B.H. Gähwiler, and R.A. McKinney. 2007. Synaptic modifications at the CA3-CA1 synapse after chronic AMPA receptor blockade in rat hippocampal slices. *J. Physiol.* 581:129–138. http://dx.doi.org/10.1113/jphysiol.2006.120550

Michalon, A., K. Koshibu, K. Baumgärtel, D.H. Spirig, and I.M. Mansuy. 2005. Inducible and neuron-specific gene expression in the adult mouse brain with the rtTA2S-M2 system. *Genesis.* 43:205–212. http://dx.doi.org/10.1002/gene.20175

Mizuno, K. 2013. Signaling mechanisms and functional roles of cofilin phosphorylation and dephosphorylation. *Cell. Signal.* 25:457–469. http://dx.doi.org/10.1016/j.cellsig.2012.11.001

Ni, Y., J. Sinnett-Smith, S.H. Young, and E. Rozengurt. 2013. PKD1 mediates negative feedback of PI3K/Akt activation in response to G protein-coupled receptors. *PLoS ONE.* 8:e73149. http://dx.doi.org/10.1371/journal.pone.0073149

Okamoto, K., T. Nagai, A. Miyawaki, and Y. Hayashi. 2004. Rapid and persistent modulation of actin dynamics regulates postsynaptic reorganization underlying bidirectional plasticity. *Nat. Neurosci.* 7:1104–1112. http://dx.doi.org/10.1038/nn1311

Olayioye, M.A., S. Barisic, and A. Hausser. 2013. Multi-level control of actin dynamics by protein kinase D. *Cell. Signal.* 25:1739–1747. http://dx.doi.org/10.1016/j.cellsig.2013.04.010

Oster, H., D. Abraham, and M. Leitges. 2006. Expression of the protein kinase D (PKD) family during mouse embryogenesis. *Gene Expr. Patterns.* 6:400–408. http://dx.doi.org/10.1016/j.modgep.2005.09.006

Penzes, P., and M.E. Cahill. 2012. Deconstructing signal transduction pathways that regulate the actin cytoskeleton in dendritic spines. *Cytoskeleton (Hoboken).* 69:426–441. http://dx.doi.org/10.1002/cm.21015

Pontrello, C.G., and I.M. Ethell. 2009. Accelerators, brakes, and gears of actin dynamics in dendritic spines. *Open Neurosci J.* 3:67–86. http://dx.doi.org/10.2174/1874082000903020067

Quassollo, G., J. Wojnacki, D.A. Salas, L. Gastaldi, M.P. Marzolo, C. Conde, M. Bisbal, A. Couve, and A. Cáceres. 2015. A RhoA signaling pathway regulates dendritic Golgi outpost formation. *Curr. Biol.* 25:971–982. http://dx.doi.org/10.1016/j.cub.2015.01.075

Quinlan, E.M., and S. Halpain. 1996. Postsynaptic mechanisms for bidirectional control of MAP2 phosphorylation by glutamate receptors. *Neuron.* 16:357–368. http://dx.doi.org/10.1016/S0896-6273(00)80053-7

Racz, B., and R.J. Weinberg. 2006. Spatial organization of cofilin in dendritic spines. *Neuroscience.* 138:447–456. http://dx.doi.org/10.1016/j.neuroscience.2005.11.025

Rácz, B., and R.J. Weinberg. 2013. Microdomains in forebrain spines: an ultrastructural perspective. *Mol. Neurobiol.* 47:77–89. http://dx.doi.org/10.1007/s12035-012-8345-y

Rémillard-Labrosse, G., C. Mihai, J. Duron, G. Guay, and R. Lippé. 2009. Protein kinase D-dependent trafficking of the large Herpes simplex virus type 1 capsids from the TGN to plasma membrane. *Traffic.* 10:1074–1083. http://dx.doi.org/10.1111/j.1600-0854.2009.00939.x

Rex, C.S., L.Y. Chen, A. Sharma, J. Liu, A.H. Babayan, C.M. Gall, and G. Lynch. 2009. Different Rho GTPase-dependent signaling pathways initiate sequential steps in the consolidation of long-term potentiation. *J. Cell Biol.* 186:85–97. http://dx.doi.org/10.1083/jcb.200901084

Rust, M.B., C.B. Gurniak, M. Renner, H. Vara, L. Morando, A. Görlich, M. Sassoè-Pognetto, M.A. Banchaabouchi, M. Giustetto, A. Triller, et al. 2010. Learning, AMPA receptor mobility and synaptic plasticity depend on n-cofilin-mediated actin dynamics. *EMBO J.* 29:1889–1902. http://dx.doi.org/10.1038/emboj.2010.72

Segal, M. 2010. Dendritic spines, synaptic plasticity and neuronal survival: activity shapes dendritic spines to enhance neuronal viability. *Eur. J. Neurosci.* 31:2178–2184. http://dx.doi.org/10.1111/j.1460-9568.2010.07270.x

Sharma, S., S. Rakoczy, and H. Brown-Borg. 2010. Assessment of spatial memory in mice. *Life Sci.* 87:521–536. http://dx.doi.org/10.1016/j.lfs.2010.09.004

Star, E.N., D.J. Kwiatkowski, and V.N. Murthy. 2002. Rapid turnover of actin in dendritic spines and its regulation by activity. *Nat. Neurosci.* 5:239–246. http://dx.doi.org/10.1038/nn811

Steinberg, S.F. 2012. Regulation of protein kinase D1 activity. *Mol. Pharmacol.* 81:284–291. http://dx.doi.org/10.1124/mol.111.075986

Wang, Y., F. Shibasaki, and K. Mizuno. 2005. Calcium signal-induced cofilin dephosphorylation is mediated by Slingshot via calcineurin. *J. Biol. Chem.* 280:12683–12689. http://dx.doi.org/10.1074/jbc.M411494200

Wang, N., P. Su, Y. Zhang, J. Lu, B. Xing, K. Kang, W. Li, and Y. Wang. 2014. Protein kinase D1-dependent phosphorylation of dopamine D1 receptor regulates cocaine-induced behavioral responses. *Neuropsychopharmacology.* 39:1290–1301. http://dx.doi.org/10.1038/npp.2013.341

Wheal, H.V., C. Bernard, J.E. Chad, and R.C. Cannon. 1998. Pro-epileptic changes in synaptic function can be accompanied by pro-epileptic changes in neuronal excitability. *Trends Neurosci.* 21:167–174. http://dx.doi.org/10.1016/S0166-2236(97)01182-X

Xu, P., K.M. Rosen, K. Hedstrom, O. Rey, S. Guha, C. Hart, and G. Corfas. 2013. Nerve injury induces glial cell line-derived neurotrophic factor (GDNF) expression in Schwann cells through purinergic signaling and the PKC-PKD pathway. *Glia.* 61:1029–1040. http://dx.doi.org/10.1002/glia.22491

Yuste, R. 2010. Dendritic spines. MIT Press, Cambridge. 264 pp. http://dx.doi.org/10.7551/mitpress/9780262013505.001.0001